SIMULATION OF FATIGUE CRACK GROWTH IN FRICTION STIR WELDED JOINTS IN 2024-T351 AL ALLOY

Amirreza Fahim Golestaneh[1*], Aidy Ali[1], Wong Shaw Voon[1], Faizal Mustapha[2] and Mehdi Zadeh Mohammadi[1]

Abstract

The aim of the present work is to predict the fatigue life of friction stir welded joints in 2024-T351 Al alloy using the finite element method in the framework of fracture analysis code for two-dimensions (FRANC2D/L). The simulation was conducted under linear elastic fracture mechanics, based on Paris' model and maximum tensile stress and displacement correlation methods were applied to calculate the crack direction and stress intensity factor, respectively. One strategy has been presented, how crack propagation was investigated based on the corresponding Paris constants for each FSW zone. Numerical results were validated with experimental and analytical work.

Keywords: Simulation, finite element method, fatigue crack growth, Paris model, friction stir welding

Introduction

Friction stir welding (FSW) is a type of solid state welding, invented in 1991 by The Welding Institute (TWI) in Cambridge UK, which involves a joining process using no filler materials (Fratinia and Zuccarellob, 2006; Scialpi *et al*., 2007). In FSW process, a threaded or non-threaded pin installed on a cylindrical tool, approaches the joint line of two butted plates while, rotating quickly and is inserted into the plates. Then pin starts to translate along the joint line and the generated frictional heat softens the material. Pin rotation deforms both plate materials plastically and drags some amount of materials from the front to the backside, effectively stirring them as shown in Figure 1. The FSW joint has a V-shaped welded area that consists of five different sub-areas called (1) the nugget zone (NZ), (2) the flow arm zone (FAZ), (3) the thermomechanically affected zone (TMAZ), (4) the heat affected zone (HAZ), and (5) the parent zone (PZ), as shown in Figure 2 (Ali *et al*., 2006; Fratinia and Zuccarellob, 2006).

[1] *Department of Mechanical and Manufacturing Engineering, Faculty of Engineering, University Putra Malaysia, 43400 Serdang, Selangor, Malaysia. Tel.:006-0122749592; E-mail: gs16938@ mutiara.upm.edu.my*

[2] *Department of Aerospace Engineering, Faculty of Engineering, University Putra Malaysia, 43400 Serdang, Selangor, Malaysia.*

[*] *Corresponding author*

One of the significant problems with FSW joints that has attracted intensive study is fatigue crack behavior and propagation through the welded joint (Lomolinoa *et al*., 2005; Ali *et al*., 2006). Ingraffea *et al*. (1987) was one of the first who attempted to simulate the crack growth in two-dimension (2-D) and under the mixed-mode condition, applying the boundary element method (BEM). In the case of a two-dimensional simulation, the crack is assumed to be a surface crack that propagates in two directions, and advancement through the thickness is not considered. Xiang *et al*. (2003) used multi-region BEM to investigate fatigue crack behavior in the 3-D case of a welded T joint specimen. Multiple fatigue crack propagation under linear elastic fracture mechanics (LEFM) for the 2-D case was simulated by Yan (2007) using BEM.

In that work, the maximum principle stress criterion was used to predict the crack growth direction, and Paris' model was extended to cover the crack propagation process for a mixed-mode multiple cracks problem. Cosenza *et al*. (2004) worked on simulation of a cold extrusion die, using Object Solid Modeler (OSM) for modeling the die, and FRANC3D for the purpose of analyzing the crack propagation based on the Paris' model. Fatigue crack behavior of a fan blade attachment in an aircraft turbine engine under centrifugal and aerodynamic loading was simulated by Barlow and Chandra (2005) as a 3-D case applying FRANC3D. In that work, due to the complex blade attachment geometry and complicated loading condition, a mixed-mode loading condition was considered. Barlow and Chandra (2005) employed the
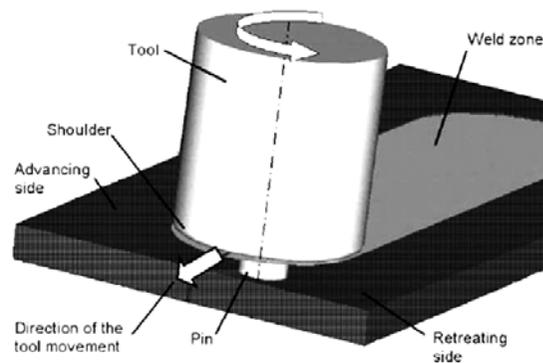
Figure 1. Schematic illustrstion of FSW butt joint (Scialpi *et al*., 2007)
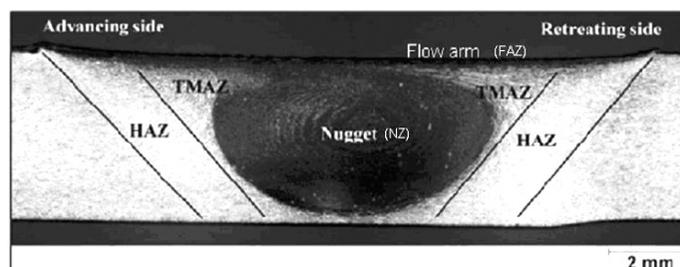
Figure 2. FSW microtructure zones (Lomolinoa *et al*., 2005)

maximum tangential stress criterion in order to predict crack growth direction and the Newman-Forman equation to calculate the growth rate.

As briefly reported above, previous work represents extensive research on crack propagation through one material with homogeneous properties, however the main target here was to study the fatigue crack behavior through the FSW joint consisting of different zones with different material characteristics. The numerical study was carried out by means of finite element method (FEM), in the workspace of FRANC2D/L and based on Paris model. Finally the fatigue lifetimes of the FSW joint were predicted for various loading conditions and represented in the frame of S-N curve. The numerical simulation results were validated with the performed experiments. The numerical predictions based on Paris model were compared with the analytically calculated lifetimes by Hobsson-Brown model (Ali *et al.*, 2008).

Simulation Process

The simulation work in this study consists of two individual processes: (1) modeling and meshing, which was carried out by CASCA software, (2) simulating and analyzing, by FRANC2D/L. This software is able to simulate layered structures in addition to crack propagation through planar (plane stress, plane strain, and axisymmetric) structures.

Modeling and Meshing the Specimen Geometry

The specimen was modeled and meshed as a two-dimensional rectangular plate with a size of 60 x 20 mm in dimensions, by CASCA. The model geometry was divided into some subregions to represent the FSW zones at both sides of the plane join line (PJL). Figure 3 shows the arrangement and dimensions of the welding zones along the model. Due to FRANC2D/L is compatible with second-degree elements (six-node triangular and eight-node quadrilateral elements) in this work eight-node quadrilateral element, which is more suitable for covering the rectangular geometry, was used. In addition displacement equations of eight-node elements are the function of more number of nodal displacements, compared with the six-node elements which provide more accuracy. Figure 3 illustrates the model geometry, covered by 1,880 elements including 21,364 nodes.
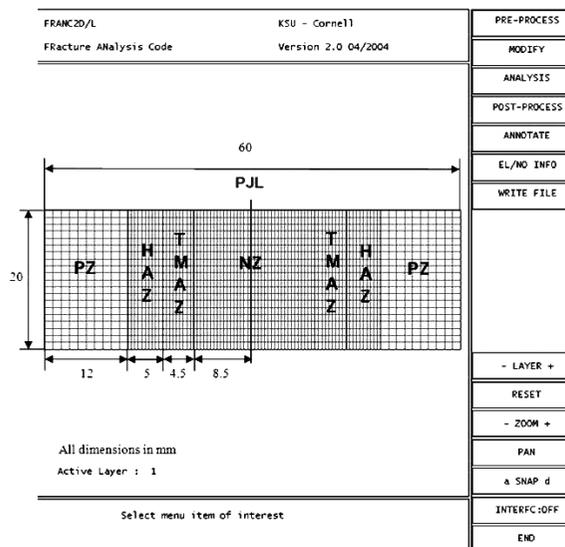
Figure 3. Specimen geometry covered by mesh elements

Analysis and Simulation

In this research, in order to verify the applied methods and strategies, the entire crack growth process through the FSW zones for one loading condition (270 MPa Max applied stress) was simulated and validated step-by-step. Then the same procedure was followed for other loading conditions in order to predict fatigue lifetimes of the FSW joint.

Problem Type

The plane stress condition was applied to the simulation in order to simplify the effect of thickness and concentrate the analysis on the crack propagation in two dimensions along the model surface.

Material Properties

Four materials with different properties were considered here in order to represent various welding zones within the model. In other words FSW zones were introduced to the model by attributing the material properties of the zones to the mesh elements. The Von Mises criterion was set for all of the zones with the mechanical properties and stress-strain relationship shown in Tables 1 and 2. Although Young's modulus (E) and Poisson's ratio (v) are the same for the zones, the hardening modulus (H) and exponent (n) vary along the welding. This variation can be attributed to the performed heat treatment. Based on the strong effect of hardness and residual stress characteristics on the fatigue behavior of the crack (Lomolinoa *et al.*, 2005; Fersini and Parondi, 2007), here variations of hardness and residual stress characteristics along the welding zones were considered as shown in Table 1.

Table 1. Material properties of FSW zones

FSW regimes	NZ	TMAZ	HAZ	PZ
Young's modulus (GPa)	68.00	68.00	68.00	68.00
Poisson's ratio 0.33	0.33	0.33	0.33	
Yield stress (MPa)	350.00	272.00	448.00	370.00
Hardening constant	-	800.00	719.00	770.00
Hardening exponent	-	0.1266	0.05546	0.086
Hardness (Hv1)	142.00	118.00	167.00	132.00
Residual stress (MPa)	-41.00	95.00	-20.00	0.00

Table 2. Stress-strain data of FSW zones

PZ		HAZ		TMAZ		NZ	
Strain	Stress (MPa)	Strain	Stress (MPa)	Strain	Stress (MPa)	Strain	Stress (MPa)
0.0003	20	0.00040	25	0.00070	50.34	0.00044	30.43
0.0006	40	0.00060	35	0.00123	75.86	0.00080	51.30
0.0009	45	0.00100	58	0.00160	106.90	0.00120	69.56
0.0014	90	0.00126	83	0.00200	131.03	0.00150	91.30
0.0021	125	0.00150	95	0.00310	186.21	0.00210	130.43
0.0034	220	0.00200	130	0.00450	268.96	0.00320	186.95
0.0050	300	0.00280	175	0.00570	331.03	0.00430	286.96
0.0058	320	0.00438	280			0.00550	331.91
0.0084	440	0.00558	330				
0.0120	487	0.00898	480				
		0.01166	540				

Loading Process

For the first time, Elber (1974) showed, the existence of residual stress within the plastic wake along the crack faces, keeps the crack faces close for the significant portion of the cycles. Many studies have investigated the crack closure effects on fatigue crack growth (Alizadeh *et al.,* 2007; Fersini and Parondi, 2007). The obtained results represented a reduction in the effective stress intensity factor range (ΔK_{eff}), which guarantees more accurate fatigue life estimation. In the present work, in order to take the effects of residual stress and crack closure into account, the effective stress range ($\Delta\sigma_{eff}$) was calculated as:

$$\Delta\sigma_{eff} = (\sigma_{max} + \sigma_{res}) - \sigma_{op} \quad \text{if} \tag{1}$$

$$\sigma_{min} + \sigma_{res} \leq \sigma_{op}$$

else

$$\Delta\sigma_{eff} = (\sigma_{max} - \sigma_{min}) \tag{2}$$

where σ_{max} is the maximum applied stress, σ_{min} is the minimum applied stress, σ_{res} denotes residual stress, and σ_{op} represents opening stress value. It is worth noting that whenever the maximum applied stress exceeds the material yield strength, some amount of residual stress is released as the result of plastic deformation. In this research, for the case when the specimen is loaded by 270 MPa Max stress, the maximum and minimum stresses after incorporating the residual stress ($\sigma_{max+res}, \sigma_{min+res}$) are:

$$\sigma_{max+res} = \sigma_{max} + \sigma_{res} = 270 + 96$$

$$= 366 \quad MPa$$

$$\sigma_{min+res} = \sigma_{max} R + \sigma_{res} = 27 + 96$$

$$= 123 \quad MPa \tag{3}$$

where $R = 0.1$ represents the stress ratio, which is the proportion of minimum stress to maximum stress. Due to maximum stress exceeds the yield strength of TMAZ (272 MPa), the residual stress relaxation was incorporated as follows:

$$\frac{366}{E} = \frac{Max\sigma_{rex}}{E} + \left(\frac{Max\sigma_{rex}}{H}\right)^n \Rightarrow$$

$$\frac{366}{68000} = \frac{Max\sigma_{rex}}{68000} + \left(\frac{Max\sigma_{rex}}{800}\right)^{0.1266}$$
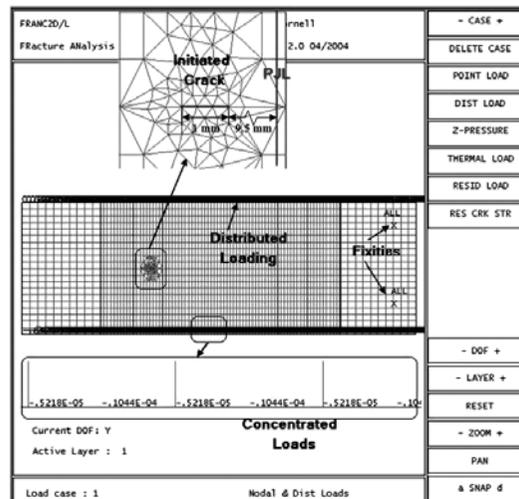
Figure 4. Loading, initiated crack, and applies constraints to the model

$$\Rightarrow Max\sigma_{rex} = 318 \qquad MPa \qquad (4)$$

where $Max\sigma_{rex}$ is the maximum stress after incorporating the relaxation. Therefore the new value of minimum stress can be calculated as $Min\sigma_{rex} = \sigma_{min+res} - (366 - 318) = 75$ MPa. According to equation (1) and $\sigma_{op} = 110$ MPa, which was considered independent of the crack length for different loading conditions, the effective stress range is $\Delta\sigma_{eff} = Max\sigma_{rex} - \sigma_{op} = 208$ MPa. Finally the calculated value of loading was applied along the two opposite edges of the model as distributing loading, however the load is attributed to the elements nodes as the concentrated loading by FRANC2D/L. Figure 4 represents the model under applied distributed loading. The equivalent concentrated loads which are attributed to the elements nodes are shown in the same Figure.

Boundary Conditions

In the present research, two individual fixities were applied to two nodes on the opposite sides of the initiated crack in order to constrain the specimen in all directions. See Figure 4. The constraints have been embedded to the right side of the model where they have less influence on the initiated crack. Figure 5 illustrates the negligible effect of the fixities on the existing crack.

Crack Initiation

Previous research confirms the intense effects of hardness and residual stress on crack initiation how, a decrease in the hardness characteristic leads to a decrease in fatigue threshold, and consequently, crack initiation is facilitated. Residual stress has a direct influence on crack initiation that high tensile residual stress enhances crack initiations (Bussu and Irving, 2003; Lomolinoa *et al.*, 2005). Therefore here the initial crack was introduced in TMAZ with the lowest hardness (118 Hv1) and with the highest residual stress of 96 MPa. The right and left tips of the crack were 9.5 and 10.5 mm away from PJL as illustrated in Figure 4.

In this work, first the entire crack propagation process was modeled in detail through the FSW zones for loading condition of 270 MPa Max stress. Therefore the initial crack with a
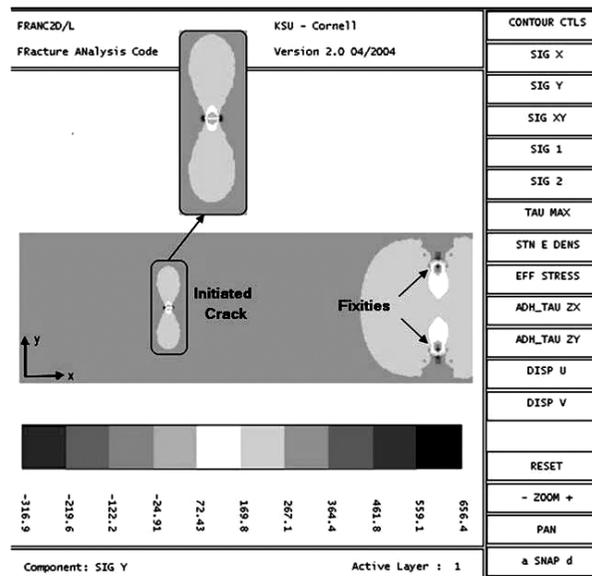
Figure 5. Stress distribution within the specimen in Y direction for the 270 MPa Max stress

length of 1 mm was introduced into the TMAZ. The smallest initial crack size identified by the replication work, for the stress condition of 270 MPa Max applied stress, was about 0.112 mm, however this value escalated to 0.62 mm for the 300 MPa. Therefore in the simulation the fatigue lifetimes were predicted by considering the initial crack with the size of 0.2 mm in TMAZ for high cycle fatigue (HCF) (loading conditions below 300 MPa Max applied stress) and 1 mm initial crack for LCF (loading conditions above 300 MPa Max applied stress) conditions.

Crack Propagation

Although the performed research confirms the identical results of different methods for calculating the crack growth direction and stress intensity factors, here, the maximum tensile stress method (Xiang et al., 2003; Scialpi et al., 2007) and the displacement correlation technique (Scialpi et al., 2007; Yan, 2007) were employed successively.

The incremental crack growth length (Δa) is one of the factors that plays a significant role in accuracy of the propagation results and has attracted much attention. The incremental crack growth length has been reported as 0.1 mm by Alizadeh et al. (2007) and Simandjuntak et al. (2006) in their work. However, Wang et al. (1999) considered this factor to be two times larger than that and he used $\Delta a = 0.20$ mm. In this work, the crack increment was considered to be 0.25 mm, which provides the required accuracy. Figure 6 illustrates the crack propagation and mesh refinement at HAZ and PZ.

Crack Growth Model

In this study, Paris' model was used, incorporating the effects of residual stress, crack closure, and stress relaxation. This model uses the LEFM to predict the stable fatigue crack growth rate within the region II, as shown in Figure 7(a). The LEFM assumes a small plastic region around the crack tip which involves that the material does not go under entire yielding condition. However, for the elastic-plastic material with the cyclic stress-strain behavior shown in Figure 7(b), even if the maximum applied stress of the cyclic loading exceeds the material yield strength, LEFM can still be applied. In fact
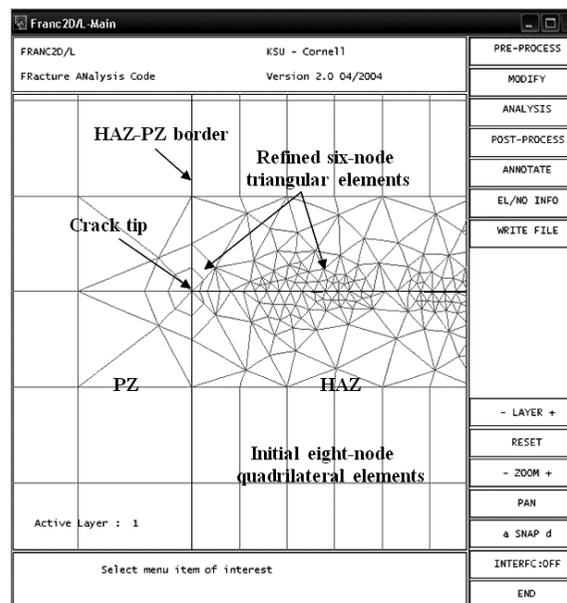
Figure 6. The initial and refined mesh elements after crack propagation

although the stress exceeds the yield strength, loading and unloading the material under the cyclic loading will increase the material yield strength up to the applied stress, regarding to the strain hardening phenomenon and therefore yielding is constrained to the small area around the crack tip (Zhang *et al.*, 1992; Corbin and Wilkinson, 1993; Ragab and Bayoumi, 1999; Rodopoulos *et al.*, 2003; Dusicka *et al.*, 2007). Working with Paris' model involves setting two constants, C and m, which are placed in the equation as shown below:

$$\frac{da}{dN} = C\left(\Delta K_{eff}\right)^m \qquad (5)$$

where *C* and *m* are material properties, obtained experimentally (Xiang *et al.*, 2003; Scialpi *et al.*, 2007; Fulland *et al.*, 2008) and ΔK_{eff} denotes effective stress intensity factor range. The values of the Paris constants have been measured through experiments and presented by Ali *et al.* (2008), but in that study, he assumed one identical value of *C* and *m* for all of the FSW zones. Two strategies were considered in this work in order to first obtain different values of Paris' constants for different welding zones, and second, to attribute these various constants to the corresponding zones. Different values of Paris' constants for the present work were calculated by applying a linear regression to
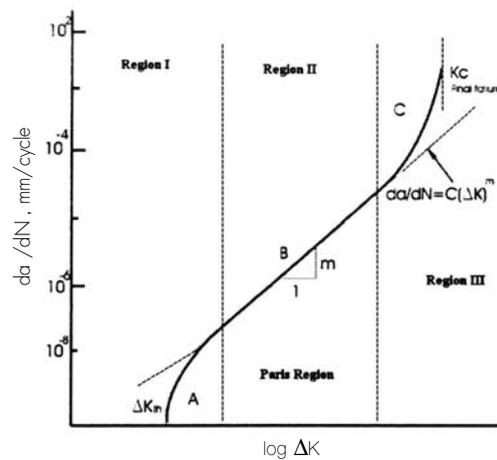
(a)
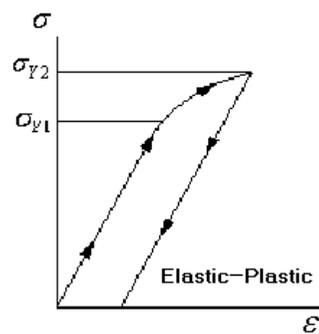
(b)

**Figure 7.   (a) Schematic illustration of the fatigue crack growth within different regions
                (b) Stress-Strain behavior of the Elastic-Plastic material under cyclic loading**

the constants obtained by Bussu and Irving (2003) for each zone and the constants obtained by Ali *et al.* (2008) only for PZ. Table 3 shows the values of C and m.

Previous work has presented various formulas for calculating the ΔK_{eff}, (Grestle, 1968; Lie *et al.*, 2000; Tanaka, 1974). In this work the ΔK_{eff} was determined using the Tanaka (1974) formula as following:

$$\Delta K_{eff} = \left(\Delta K_I^4 + 8\Delta K_{II}^4 + \frac{8K_{III}^4}{1-\nu} \right)^{1/4} \qquad (6)$$

where ΔK_I, ΔK_{II}, and ΔK_{III} are successively stress intensity factors of modes I, II, and III. The values of stress intensity factor for mode I and II were obtained numerically using displacement correlation technique as below:

$$K_I = \frac{2G}{(3-4\nu)+1} \sqrt{\frac{\pi}{2L}} \left[4v_d - v_e - 4v_b + v_c \right]$$

$$K_{II} = \frac{2G}{(3-4\nu)+1} \sqrt{\frac{\pi}{2L}} \left[4u_d - u_e - 4u_b + u_c \right] \quad (7)$$

where G is the shear modulus and u and v denote the displacements of the nodes b, c, d,

and e in Figure 8. Note that $\Delta K_{III} = 0$ in accordance with the applied loading and boundary condition shown in the Figure 4. Figure 9. presents the maximum values of stress intensity factor of mode I and II ($K_{I, max}$ and $K_{II, max}$) for the initial crack under 270 MPa maximum applied stress. Therefore $\Delta K_I = (1 - R) K_{I, max} = 11.96$ $MPa\sqrt{m}$ and $\Delta K_{II} = (1 - R) K_{II, max} = 2.96 \times 10^{-3}$ $MPa\sqrt{m}$ for $R = 0.1$. Substituting the calculated values for ΔK_I and ΔK_{II} in Equation 6 yields $\Delta K_{eff} = 11.961$ $MPa\sqrt{m}$ awhich is very close to the value of the ΔK_I, implying the intense influence of mode I. The fatigue crack growth direction was predicted using the maximum principle stress criterion, incorporating the mixed-mode condition. Based on this criterion the crack propagation direction from one point on the crack front is calculated in the local coordinate system as shown in Figure 8 by:

$$\tan\frac{\theta_o}{2} = \frac{1}{4} \left[\frac{\Delta K_I}{\Delta K_{II}} - \sqrt{\left(\frac{\Delta K_I}{\Delta K_{II}} \right)^2 + 8} \right]$$

$$= \frac{-2\Delta K_{II}}{\Delta K_I + \sqrt{(\Delta K_I)^2 + 8(\Delta K_{II})^2}} \qquad (8)$$

Table 3. Paris' constants from Bussu and Irving (2003), Ali *et al*. (2008) and regression calculation for FSW zones of 2024-T351 Al alloy

FSW regimes	Paris'model constants	Bussu-Irving experiments	Ali experiments	Regression calculations
NZ	C *(cycle)$^{-1}$*	2.02345×10^{-10}	2.85×10^{-12}	2.8338×10^{-12}
	m	3.106	2.94	3.80
TMAZ	C *(cycle)$^{-1}$*	3.987×10^{-10}	2.85×10^{-12}	5.5837×10^{-12}
	m	2.254	2.94	2.76
HAZ	C *(cycle)$^{-1}$*	8.41×10^{-11}	2.85×10^{-12}	1.1778×10^{-12}
	m	2.28	2.94	2.79
PZ	*(cycle)$^{-1}$*	2.035×10^{-10}	2.85×10^{-12}	2.85×10^{-12}
	m	2.4	2.94	2.94

where θ_0 is the crack growth direction. Substituting the obtained values of ΔK_I and ΔK_{II} into Equation 8, yields $\theta_0 = -0.5 \times 10^{-3}$ rad which confirms the straight crack propagation under the dominant effect of mode I at the crack growth commencement. However the influences of modes II and III in crack propagation decreases quickly in comparison with mode I, as the crack grows (Bowness and Lee, 1998). Therefore the present work was studied under the pure mode I and the effect of mode II was simplified without loss of accuracy.

FRANC2D/L has its limitations to work only based on one value for each C and m (Paris' constants). Therefore here, during crack propagation within each zone, the program was set to the corresponding Paris' constants and the number of cycles was calculated based on the number of cycles at the end of previous zone as the origin for counting the cycles, as illustrated in Figures 10.

Results and Discussion

First, we note that FRANC2D/L has the capability to simulate and predict fatigue crack behavior under stable propagation condition within region II and based on Paris' model. This model is basically established for investigating an edge crack; however, in order to cope with an internal crack placed within the specimen, the internal crack is considered as two individual edge cracks in opposite directions. Then, Paris' model is applied to one of them, and finally the same results are considered for the other edge crack. This method is valid whenever the same fatigue behavior can be attributed to both tips of an internal crack, which means that both of the tips propagate within the same material with the same properties. Therefore, for the present work in which the FSW specimen was initiated with an internal crack within the TMAZ, the explained method can be applied up to 46,000 cycles, where the right crack tip touches the boundary between TMAZ and NZ. While the crack tip crosses the border and enters NZ, the crack propagation rate will rise significantly and the right tip will speed along the NZ however the left tip advances slowly through the other zones. Figure 10 represents fast growth of the right tip within the NZ compared with the left tip propagation through the TMAZ, HAZ, and PZ.

Due to the right side of the internal crack can reach any arbitrary sizes before the left side, the number of cycles in which the internal crack reaches a particular size is obtained based on the propagation of the left crack tip. Therefore,
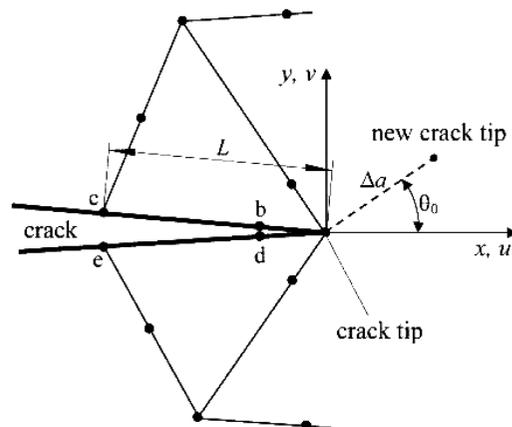
Figure 8. Loacal coordinate system at the crack tip (Xiang *et al*., 2003)

the fatigue behavior of the internal crack was attributed to the left tip.

Figure 11 represents the entire crack propagation through the specimen, which was initiated with 1 mm crack at TMAZ, up to the length of 14.5 mm after about 190,000 cycles. This figure compares the results of numerical simulation method with the analytical (Ali *et al*., 2008) one. As it is observed the crack propagation process accelerates along the welding zones and the slope of the curve decreases. The crack behavior is intensely affected by the variation of hardness and residual stress along the zones. Increase in hardness from the TMAZ (118 Hv1)

Figure 9. KI and KII of the initial crack under 270 MPa applied stress
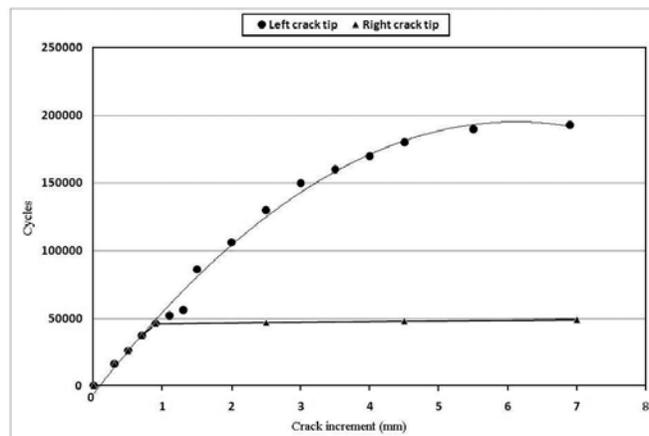
Figure 10. Number of cycles versus crack increment

Figure 10. Number of cycles versus crack increment

to the highest value of 167 (Hv1) at the next zone (HAZ) supports higher crack growth rate (decrease in the slope of the curve) from TMAZ to HAZ. However due to the decrease in hardness after HAZ, the hardness characteristic contrasts with the observed increase in the crack propagation rate along PZ. The increase in crack growth rate within the PZ compared with the HAZ is attributed to the lower residual stress (negative residual stress) within the HAZ. During crack propagation phenomenon the crack length increases which causes higher crack growth rate as described in equations (5) and (6):

$$\Delta K \propto \Delta \sigma \sqrt{\pi a} \tag{9}$$

where ΔK is stress intensity range, $\Delta \sigma$ is stress range, and a denotes half of the internal crack length. Therefore, hardness variation and the crack growth phenomenon both have the positive impact on the increase in crack growth rate, within the HAZ compared with the TMAZ. Although hardness has a negative effect on the increase of crack growth rate along PZ, residual stress and crack growth phenomenon support higher growth rate through PZ compared with the HAZ.

Figure 11 confirms the employed methods in the present work, and therefore these applied strategies can be extended for other loading conditions in order to simulate and predict fatigue lifetimes, and consequently, the S-N curve of the FSW joint.

As explained before, in this work, the initial cracks are long enough so that, crack initiation through region I is not considered or in other words fatigue life is not influenced by the crack initiation process through this region.

Table 4 confirms the high rate of crack growth for PZ as compared with HAZ, which validates when the crack approaches region III, the effect of crack propagation on lifetime decreases. Therefore, ignoring the crack growth within region III and establishing the calculations based on Paris' model does not influence the fatigue lifetime results. Figure 12 shows predicted fatigue lifetimes of FSW joint, based on numerical simulation method, which were validated with experiments. The results of the previous analytical study (Ali *et al.*, 2008) have been represented for the comparison purpose. The predicted results present a good agreement with acceptable accuracy with the experiments which implies the capability of the Paris model to predict the fatigue crack propagation within the FSW joint. However the predicted lifetimes are higher than the test results. One of the effective factors in the fatigue crack behavior is material
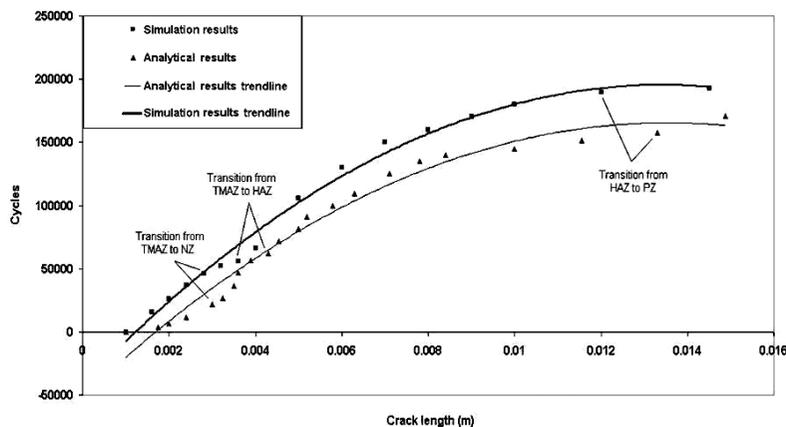
Figure 11. The entire crack propagation though the specimen based on simulation and analytical methods for the 270 MPa Max stress

characteristics like material microstructure which was not considered in this simulation due to the FRANC2D/Llimitations. In fact microstructure characteristic playsa stronger role in crack initiation phenomenon, compared with the propagation process in the second region, however considering this factor will improve the final results. The variation of two other effective factors (residual stress and hardness) along the each welding zone influences the fatigue lifetime and causes the observed differences between the test and simulation results. It is worth noting that every micro-region in FSW joint has different fatigue threshold, therefore higher applied loading (LCF) increases the number of short cracks which overcome the threshold stress intensity factor (K_{th}) and causes multiple crack phenomenon. Figure 12 illustrates higher agreement between the simulated and experimental results for lower applied loadings (HCF). It is worth noting that the smallest individual surface crack lengths detected by replication work were 0.112mm and 0.62mm length for 270 MPa and 300 MPa maximum stresses applied respectively. Since most cracks were initiated from defects, with the length in order of 20mm, these initial cracks for both HCF and LCF can be considered as microstructurally long cracks, which propagate within region II.

In other words although in the present study simulation was based on Paris' model which only supports the crack propagation through region II, the obtained simulation results are acceptable due to the initial crack is long enough that propagation starts through region II and fatigue life is not influenced by the crack initiation process.

The comparison between the numerically predicted lifetimes in this research and the analytically calculated ones obtained by the previous work (Ali *et al.*, 2008) confirms a high percentage of similarity between the Paris and Hobsson-Brown models for the case of fatigue crack study in FSW joint. This high agreement implies another validation of the Paris model application in the framework of FRANC2D/L for FSW.

Conclusions

1) Fatigue crack propagation through FSW joint consisting of four different zones with various characteristics was simulated by applying FEM and in the framework of FRANC2D/L. The crack behavior was studied based on Paris model incorporating the effects of residual stress, stress relaxation and crack closure concepts. The simulation showed good agreement with analytical results.
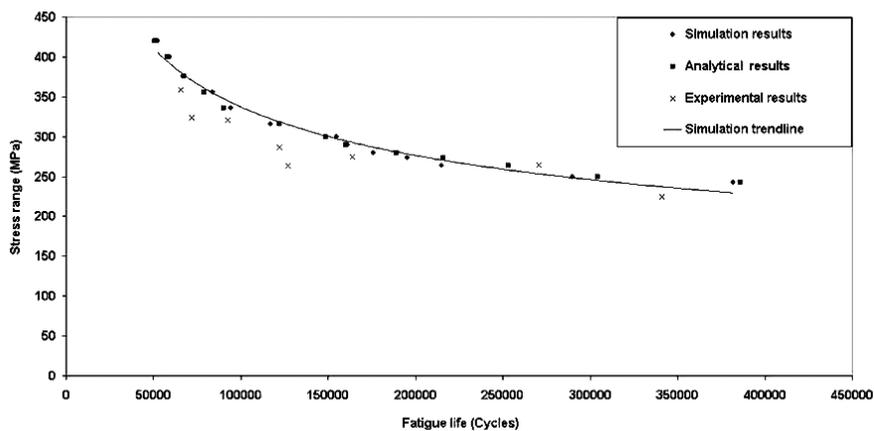
Figure 12. Fatigue life prediction of FSW joint in 2024-T351 Al alloy

Table 4. Number of cycles at the end of each FSW zone for different stress conditions

Max stress (MPa)	At TMAZ-HAZ boundary (Cycles)	At HAZ-PZ boundary (Cycles)	Last propagation step (Cycles)
270.0	88,000	378,000	382,000
277.8	145,000	285,000	290,000
292.5	84,000	210,000	215,000
303.6	75,000	190,000	195,000
311.0	70,000	172,000	176,000
322.0	64,000	159,000	161,000
333.0	90,000	155,000	155,000
351.0	55,000	115,000	117,000
373.0	42,500	92,500	94,000
395.0	36,000	83,000	84,000
418.0	30,000	66,000	67,000
444.0	26,000	58,000	59,000
466.0	23,500	51,500	52,500

2) Fatigue lifetimes for FSW joint of 2024-T351 Al alloy were predicted numerically and represented in the form of S-N curve. The lifetime predictions represent high accuracy with the performed experiments.

3) Paris and Hobsson-Brown models yield close predictions for the fatigue lifetime where crack growth phenomenon does not include initiation process through the region I and only consists of stable propagation within region II.

Acknowledgement

References

Ali, A., Brown, M.W., and Rodopoulous, C.A. (2008). Modeling of crack coalescence in 2024-T351 Al alloy friction stir welded joints. Int J Fatigue, 30:2,030-2,043.

Ali, A., Brown, M.W., Rodopoulos, C.A., and Gardiner, S. (2006). Characterization of 2024-T351 friction stir welding joints. J Failure Anal Prevent, 6(4):41-53.

Alizadeh, H., Simandjutak, S., Smith, D., and Pavier, M. (2007). Prediction of fatigue crack growth rates using crack closure finite element analysis. Int. J. Fatigue, 29: 1,711-1,715.

Barlow, K.W. and Chandra, R. (2005). Fatigue crack propagation simulation in an aircraft engine fan blade attachment. Int. J. Fatigue, 27:1,661-1,668.

Bowness, D. and Lee, M. (1998). Fatigue crack curvature under the weld toe in an offshore tubular joint. Int. J. Fatigue, 20:481-490.

Bussu, G. and Irving, P.E. (2003). The role of residual stress and heat affected zone properties on fatigue crack propagation in friction stir welded 2024-T351 aluminum joints. Int. J. Fatigue, 25:77-88.

Corbin, S.F. and Wilkinson, D.S. (1993). Influence of matrix strength and damage accumulation on the mechanical response of a particulate metal matrix composite. Acta Metall. Mater, 42(4):1,329-1,335.

Cosenza, C., Fratini, L., Pasta, A., and Micari,

F. (2004). Damage and fracture study of cold extrusion dies. Eng. Fract. Mech., 71: 1,021-1,033.

Dusicka, P., Itani, A.M., and Buckle, I.G. (2007). Cyclic response of plate steels under large inelastic strains. J. Constr. Steel Res., 63: 156-164.

Elber, W. (1974). Effect of shot-peening residual stresses on the fracture and crack-growth properties of D6AC steel. Fracture Toughness and Slow-Stable Cracking, ASTM STP, 559:45-58.

Fersini, D. and Parondi, A. (2007). Fatigue behavior of Al 2024-T3 friction stir welded lap joint. Eng. Fract. Mech., 74:468-480.

Fratinia, L., and Zuccarellob, B. (2006). An analysis of through-thickness residual stresses in aluminum FSW butt joints. Int. J. Mach. Tool Manu, 46:611-619.

Fulland, M., Sander, M., Kullmer, G., and Richard, H.A. (2008). Analysis of fatigue crack propagation in the frame of a hydraulic press. Eng. Fract. Mech., 75:892-900.

Grestle, W. (1986). Finite and boundary element modeling of crack propagation in two- and three-dimensions using interactive computer graphics. Cornell University.

Ingraffea, A.R., Blandford, G., and Liggett, J.A. (1987). Automatic modeling of mixed-mode fatigue and quasi-static crack propagation using the boundary element method. 4th National Symposium on Fracture, ASTM STP.

Lie, S., Xiang, Z., Wang, B., and Cen, Z. (2000). Experimental and numerical simulation of 3D fatigue crack for plate-to-plate welded joints. Int. J. Fatigue, 22:411-424.

Lomolinoa, S., Tovob, R., and dos Santos, J. (2005). On the fatigue behavior and design curves of friction stir butt-welded Al alloys. Int. J. Fatigue, 27:305-316.

Ragab, A-R.A.F., and Bayoumi, S.E.A. (1999). Engineering solid mechanics: fundamentals and applications. 2ed: Boca Raton, Fl.: CRC Press.

Rodopoulos, C.A., Romero, J.S., Curtis, S.A., de los Rios, E.R., and Peyre, P. (2003). Effect of controlled shot peening and laser shock peening on the fatigue performance of 2024-T351 aluminum alloy. JMEPEG, 12:414-419.

Scialpi, A., de Filippis, L.A.C., and Cavaliere, P. (2007). Influence of shoulder geometry on microstructure and mechanical properties of friction stir welded 6082 aluminum alloy. Mater Design, 28:1,124-1,129.

Simandjutak, S., Alizadeh, H., Smith, D.J., and Pavier, M.J. (2006). Three dimensional finite element prediction of crack closure and fatigue crack growth rate for a corner crack. Int. J. Fatigue, 28:335-345.

Tanaka, K. Fatigue crack propaagtion from a crack inclined to the cyclic tensile axis. (1974). Eng. Fract. Mech., 6:493-507.

Wang, H., Buchholz, F.G., Richard, H.A., Jagg, S., and Scholtes, B. (1999). Numerical and experimental analysis of residual stresses for fatigue crack growth. Comp. Mater Sci., 16:104-112.

Xiang, Z., Lie, S.T., Wang, B., and Cen, Z. (2003). A simulation of fatigue crack propagation in a welded T-joint using 3D boundary element method. Int. J. Pre.s Ves. Pip., 80:111-120.

Yan, X. (2007). Automated simulation of fatigue crack propagation for two-dimensional linear elastic fracture mechanics problems by boundary element method. Eng. Fract. Mech., 74:2,225-2,246.

Zhang, X., Chan, A.S.L., and Davies, G.A.O. (1992). Numerical simulation of fatigue crack growth under complex loading sequences. Eng. Fract. Mech., 42:305-321.